Ultrasound-and-microbubble-mediated Drug Delivery in Microvascular Networks

Eric Juang

A thesis

submitted in partial fulfillment of the

requirements for the degree of

Master of Science in Bioengineering

University of Washington

2017

Committee:

Mike Averkiou, Chair

Ying Zheng, co-Chair

Program Authorized to Offer Degree:

Bioengineering

University of Washington

Abstract

Ultrasound-and-microbubble-mediated Drug Delivery in Microvascular Networks

Eric King-Fu Juang

Chairs of the Supervisory Committee:
Dr. Mike Averkiou
Dr. Ying Zheng
Department of Bioengineering

In recent research, ultrasound and microbubble-mediated membrane perforation (i.e. sonoporation) has shown great promise in improving the efficacy and delivery efficiency of drugs and genetic materials to tumor cells and malignant tissues. However, the exact mechanism of sonoporation and the optimal ultrasound parameters and microbubble concentration to produce sonoporation in vivo remain unclear. Furthermore, most attempts to study sonoporation have used simple *in vitro* cell-monolayer setups that failed to capture the complex human vascular environment and the microbubble-vessel interactions seen in vivo. Therefore, there exist great needs to 1) quantitatively assess the individual effects of ultrasound parameters and microbubble concentration on producing sonoporation, and 2) develop a perfusable in vitro

microvascular model which features *in vivo*-like flow characteristics, 3D geometry, and biotransport properties.

In this work, we evaluated 1) the attenuation of ultrasound at different microbubble concentrations, 2) the behavior of microbubbles at different acoustic pressures. 3) the efficacy of sonoporation in an acoustically transparent in vitro cell-monolayer setup. Our group has also successfully developed an endothelialized 3D microvascular model that recapitulates the complex structure and flow characteristics found in vivo, and this model was used to evaluate the efficacy of sonoporation in an in vivo-like environment. Our results showed that 1) acoustic attenuation increased with microbubble concentration and was dependent on the source acoustic pressure, 2) microbubble destruction and acoustic streaming increased with acoustic pressure, number of cycles, and duty cycle, 3) repeated ultrasound pulse at acoustic pressure greater than 500 kPa could be needed to induce sonoporation in vitro, and 4) based on the sonoporation data obtained with our in vitro microvascular model, the acoustic pressure and microbubble concentration needed to induce sonoporation in vivo could be much higher than expected from the results obtained with in previous in vitro studies. Our findings underscore the importance of using in-vivo-like microvascular models to study sonoporation.

TABLE OF CONTENTS

LIST OF FIGURES

ACKNOWLEDGEMENTS

The financial support from NIH awards (1DP2DK102258 and UH2/UH3 TR000504) and Life Science Discovery Fund (3292512) is acknowledged. The experimental support from Ine De Cock, Kiet Phong, and Sara Keller is gratefully acknowledged.

Chapter 1. INTRODUCTION

Due to its safe and noninvasive nature, ultrasound has been used in a variety of diagnostic and therapeutic applications such as diagnostic sonography, flow quantification, thermal ablation, and shock wave lithotripsy. In recent years, a new ultrasound application has emerged as scientists have begun to utilize it to enhance the delivery of genetic materials (eg. plasmids, siRNA, mRNA) and chemotherapeutic agents [1-8]. This enhanced delivery is accomplished by the use of microbubbles, which are small (1-10um) gas spheres stabilized by lipid, protein, or polymeric shells [9]. While microbubbles are primarily used as ultrasound contrast agents to improve the imaging quality of perfused tissues, they have been shown to transiently perforate and permeate cellular membranes under proper acoustic conditions [10-13]. This biomechanical process is commonly referred to as sonoporation. In addition to membrane permeation, sonoporation can also trigger cellular responses such as actin cytoskeletal rearrangement and clathrin-dependent endocytosis to further facilitate drug uptake by affected cells [13-15]. Mechanistically, microbubbles expand and contract rhythmically (or cavitate) at the frequency of ultrasound. Depending on the acoustic pressure of the ultrasound pulse used, microbubble cavitation can be classified into two types: inertial cavitation and stable cavitation. Stable cavitation occurs at lower acoustic pressures, at which microbubbles exhibit low-amplitude cavitation and generate microstreaming in the surrounding fluid. Inertial cavitation occurs at higher acoustic pressures, at which microbubble exhibit non-linear, high-amplitude cavitation. Inertial cavitation often results in the implosion of microbubbles and the consequent release of shock waves and micro air jets [12-13]. Both inertial and stable cavitation contribute to sonoporation, although it remains unclear which plays a bigger role.

Despite many publications demonstrating the efficacy of various medical applications of sonoporation, quantitative characterization of the acoustic parameters (e.g. acoustic pressure, pulse duration, pulse repetition, and duty cycle) and non-acoustic parameters (e.g. microbubble concentration and microbubble size) relevant to sonoporation remains difficult and inconsistent among different reports [10, 16-21]. For instance, De cock et al. and van Rooij et al. have demonstrated that sonoporation efficiency increased with acoustic pressure, up to 500 kPa peak negative pressure, but this increase in sonoporation was accompanied by higher rates of cell death [17, 18]. Contrarily, Helfield et al. observed high sonoporation efficiency and low cell death with PNP as high as 800 kPa, although they used no pulse repetition and significantly shorter pulse cycles [19]. Still, Karfashian et al. showed high sonoporation efficiency and low cell death rate at 600 kPa with moderate pulse length and pulse repetition frequency [10]. Microbubble concentration is another major determinant of sonoporation efficiency, but similar to the case with acoustic pressure, the ideal microbubble concentration for sonoporation remains to be determined.

We reasoned that part of the inconsistencies in literature can be attributed to the shortcomings of existing sonoporation models and the absence of an in-vivo-mimicking in vitro model. In fact. previous efforts to study sonoporation in vitro have mostly used cell suspensions and transparent cell enclosures with acoustically transparent windows [10, 17-21]. Although these models are easy to produce and allow direct observation of cellular response to ultrasound and microbubbles, they fail to recapitulate important biophysical features such as blood flow, three-dimensional (3D) vascular architecture, and extracellular matrix support. Additionally, these in vitro models allow direct microbubble-cell contact, which does not occur in vivo with microbubbles moving constantly in the blood. Consequently, it is difficult to translate the

findings from in vitro experiments to in vivo application. To address the dissimilarities between in vitro models and human vasculature in vivo, our group has pioneered an 3D enthothelialized microvascular construct with perfusable vascular networks. This construct has been well-characterized in previous studies and has shown great physiological similarities with the human vasculature [22-24]. In this work, we will study sonoporation with this model.

There are three major aims to the present work: 1) to suggest effective ultrasound parameters and microbubble concentrations for sonoporation by examining acoustic attenuation and microbubble dynamics, 2) to verify the sonoporation effect of suggested parameters in a static in vitro cell culture, and lastly, 3) to explore the sonoporation effectiveness of similar or identical parameters with the in vitro microvascular model. Overall, the experiments designed for these aims should give insights into the proper acoustic and non-acoustic conditions required to produce sonoporation in vivo.

To give an overview of all the chapters in this work: in chapter 2, we will detail the materials and procedures involved in all experiments conducted; in chapter 3 and 4, we will present the results from each experiment and discuss our findings; in chapter 5, we will summarize and conclude our findings.

Chapter 2. MATERIALS AND METHODS

In this chapter, you will be given summaries of all the materials and procedures involved in this work. We begin with procedures that are relevant to most parts of this work, which include the synthesis of custom-made microbubbles (2.1) and the techniques to viral-transfect and culture GFP-labeled endothelial cells (2.2). Next, we provide information about the experiments designed to study acoustic attenuation (2.3) and microbubble dynamics (2.4). Suggested ultrasound parameters and microbubble concentration based on these experiments will be verified with the method detailed in section 2.5. Finally, we present a simplified fabrication protocol of our in vitro microvascular model (2.6) and the setup we used to study sonoporation with this model (2.7).

2.1 SYNTHESIS OF CUSTOM-MADE MICROBUBBLES

Custom-made microbubbles composed of DPPC (1,2-dipalmitoyl-sn-glycero-3-phosphocholine) (Lipoid, Ludwigshafen, Germany) and DSPE-PEG (1,2-distearoyl-sn-glycero-3-phosphoethanolamine-N-[methoxy(polyethylene glycol)-2000]) ammonium salt) (Avanti Polar Lipids Inc, Alabaster, AL, USA) in a 95:5 molar ratio were prepared with previously described method. [25]. Briefly, the synthesis of microbubbles was done in the following way: 1) a 95:5 DPPC-(DSPE-PEG) lipid mixture dissolved in chloroform ($CHCl_3$) was transferred to a round-bottom flask. 2) Using a rotary evaporator (BÜCHI, Flawil, Switzerland), chloroform was carefully evaporated such that the mixture stayed in lipid phase. 3) After chloroform was fully removed, the lipid mixture was re-dissolved in a mixture of 10% glycerol, 20% propylene glycol, and 70% deionized water. 4) After proper mixing to obtain a clear lipid solution, aliquots of this solution were transferred to 2.5ml chromatography vials, whose headspace was filled with perfluorobutane (C_4F_{10}) gas. 5) Microbubbles were activated by charging with perfluorobutane

(C_4F_{10}) gas and high-frequency shaking with VIALMIX® (Lantheus Medical Imaging, North Billerica, MA, USA) for 15s. The concentration and size of microbubbles were determined with Multisizer 3 (Beckman Coulter, Brea, California, USA). The mean diameter of our custom-made microbubbles was approximately 3 μm. Microbubble dilutions for experiments were prepared in deionized water.

2.2 VIRAL TRANSFECTION AND CULTURE OF ENDOTHELIAL CELLS

The human umbilical vein endothelial cells (HUVECs) used in some of our experiments have been viral-transfected to express green fluorescent proteins (GFP) constitutively. The GFPs were stored in the cytosol and would fluoresce green as long as the HUVECs remain viable. To briefly summarize the transfection procedures, HUVECs were incubated with hTERT lentivirus (cellomics technology, Halethorpe, MD, USA) carrying GFP transcripts for two days then purified with puromycin (2 μg/ml). Successfully transfected GFP-HUVECs were cultured in T75 cell-culture flasks (Corning inc., Corning, New York, USA) in a humidified incubator with 5% CO_2 at 37°C. Endothelial Cell Growth Medium (EGM Bullet Kit™, Lonza, Basel, Switzerland) supplemented with 2 μg/ml puromycin was used.

2.3 ACOUSTIC ATTENUATION BY MICROBUBBLES

As mentioned previously, we designed experiments to test the acoustic parameters that we believed may lead to effective sonoporation in acoustically transparent cell-culture devices, i.e. CLINIcell25® (MABIO, Tourcoing, France). Since acoustic pressure affects the amplitude and mode (inertial or stable) of microbubble cavitation as well as the radiation force exerted on the cells, it was necessary to estimate the actual acoustic pressure experienced by the cells after an incident ultrasound pulse had attenuated propagating through microbubbles. To measure acoustic

attenuation by microbubbles, we placed a microbubble-filled CLINIcell vertically in between a custom-made focused transducer (transducer frequency: 1 MHz; signal amplification at focus: 2.6; focal distance: 4cm; diameter: 2cm) and a PVDF needle hydrophone (Precision Acoustics, Dorset, UK) in a water tank (Figure 2.1). The needle hydrophone was placed close to the CLINIcell membrane and on the opposite side of the custom-made transducer, the side which a cell monolayer would be in a CLINIcell. Since ultrasound was presumed to be lossless in water, the acoustic pressure measured by the needle hydrophone was assumed to be identical to the pressure experienced by the cells. The custom-made focused transducer was connected to a function generator (Tektronix, Beaverton, OR, USA) and a RF power amplifier (Electronics & Innovation, Rochester, NY, USA); it was used to send an ultrasound pulse to the microbubble-filled CLINIcell. The transmitted pulse was received by the needle hydrophone, which records acoustic pressures as voltages. All recorded voltages were normalized to the voltage measured in a lossless (water) environment. To evaluate the trend of acoustic attenuation, the experiment was repeated for different microbubble concentrations (5×10^3, 1×10^4, 5×10^4, 1×10^5, 2.5×10^5, 5×10^5, 1×10^6, 2×10^6, 4×10^6 MBs/ml) and two acoustic pressures (100 kPa and 500 kPa). Single ultrasound pulse was used for every experiment, and the ultrasound frequency and the pulse duration was kept constant at 1 MHz and 20 cycles, respectively. The frequency of 1 MHz was selected such that most custom-made microbubbles (mean size = 3 µm) would cavitate at resonance according to the Minnaert resonance equation

$$\omega_0 = \frac{1}{R_0}\sqrt{\frac{3\gamma P_A}{\rho}} \qquad (2.1)$$

Where ω_0 is the linear resonance frequency of a microbubble, R_0 is the radius of the microbubble, γ is the adiabatic gas constant, P_A is the ambient pressure, and ρ is the density of water. The

reasoning and selection of ultrasound frequency were the same for all subsequent experiments described.

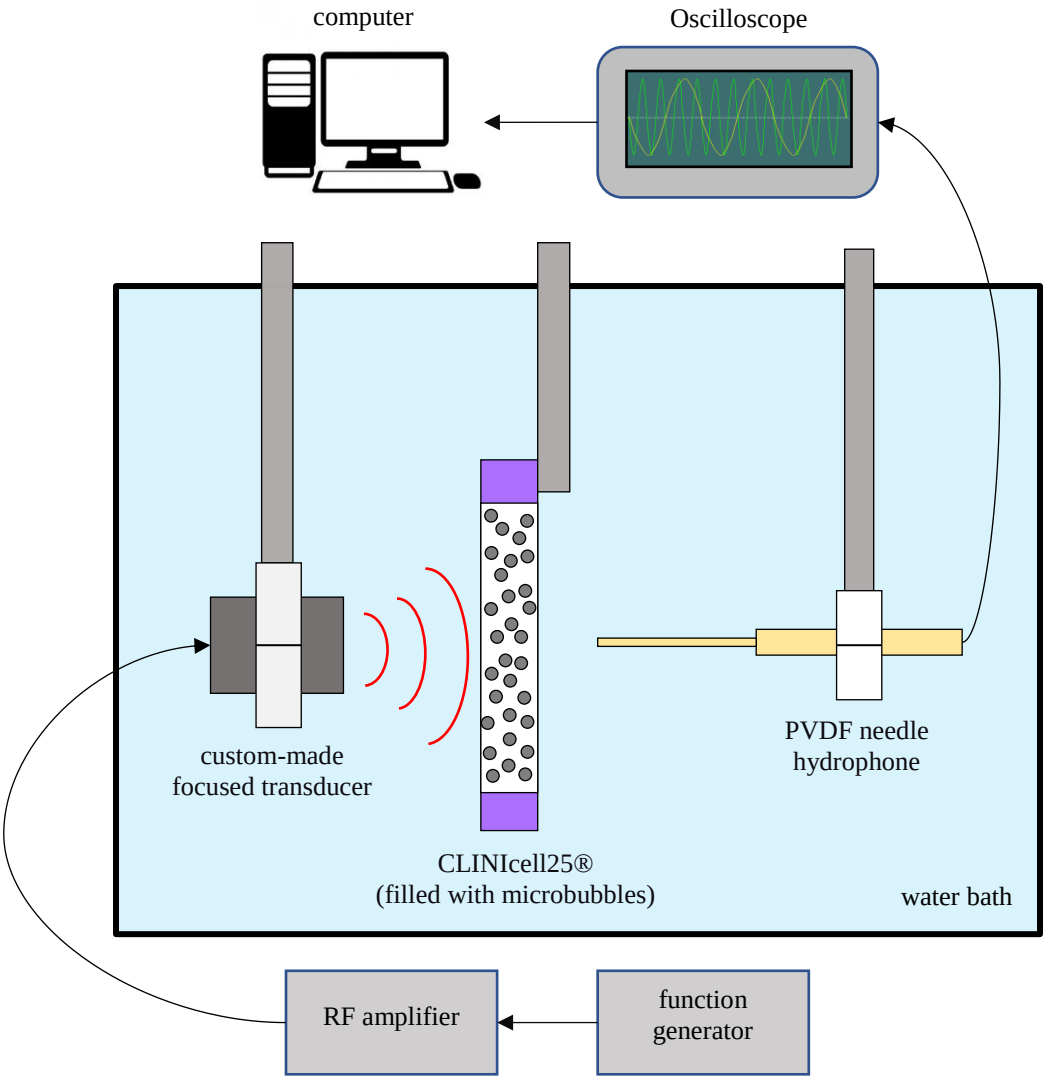

Figure 2.1. Instrument setup for measuring acoustic attenuation by microbubbles. A CLINIcell was placed vertically in between a custom-made transducer and a PVDF needle hydrophone. An ultrasound pulse sent by the custom-made transducer went through the CLINICell and was received by the needle hydrophone.

.

2.4 MICROBUBBLE DESTRUCTION AND TRANSLATION IN THE PRESENCE OF ULTRASOUND

In addition to measuring ultrasound attenuation by microbubbles, we also examined the behavior of microbubbles under the influence of different ultrasound pulses. In this experiment, we tested three acoustic pressures: 200 kPa, 500 kPa, and 1 MPa, which were all above the pressure threshold for inertial cavitation. While we expected to observe microbubble destruction at all three acoustic pressures, we also anticipated different microbubble destruction and translation patterns. We hoped to identify certain patterns that could be responsible for greater extents of sonoporation. Other than varying acoustic pressures, we also examined microbubble behaviors at different microbubble concentrations, which included 2×10^5, 4×10^5, and 2×10^6 MBs/ml. The central transducer frequency (1 MHz) and pulse duration (1000 cycles) were kept constant for all exposures.

To summarize the experimental setup, a CLINIcell was filled with microbubbles immediately prior to imaging and was placed horizontally in between a custom-made focused transducer (transducer frequency: 1 MHz; signal amplification at focus: 2.6; focal distance: 4 cm; diameter: 2 cm) and an imaging transducer (L15-7io linear array; Philips Healthcare, Bothell, WA, USA) in a water tank. A function generator (Tektronicx, Beaverton, OR, USA) was used to produce a desired acoustic signal, which was first augmented by a RF power amplifier (Electronics & Innovation, Rochester, NY, USA) then delivered to the custom-made transducer to burst an ultrasound pulse in the direction of CLINIcell. Each CLINICell was positioned at the focus of the custom-made transducer and exposed to ultrasound four times in four different areas. These areas were sufficiently far apart such that each exposure doesn't affect the distribution of microbubbles in other exposed areas. The pulse residual which travelled through the microbubble-filled CLINICell was received by the

imaging transducer on the opposite end of the CLINICell and were relayed to an imaging unit (iU-22; Philips Healthcare, Bothell, WA, USA) to produce B-mode image recordings.

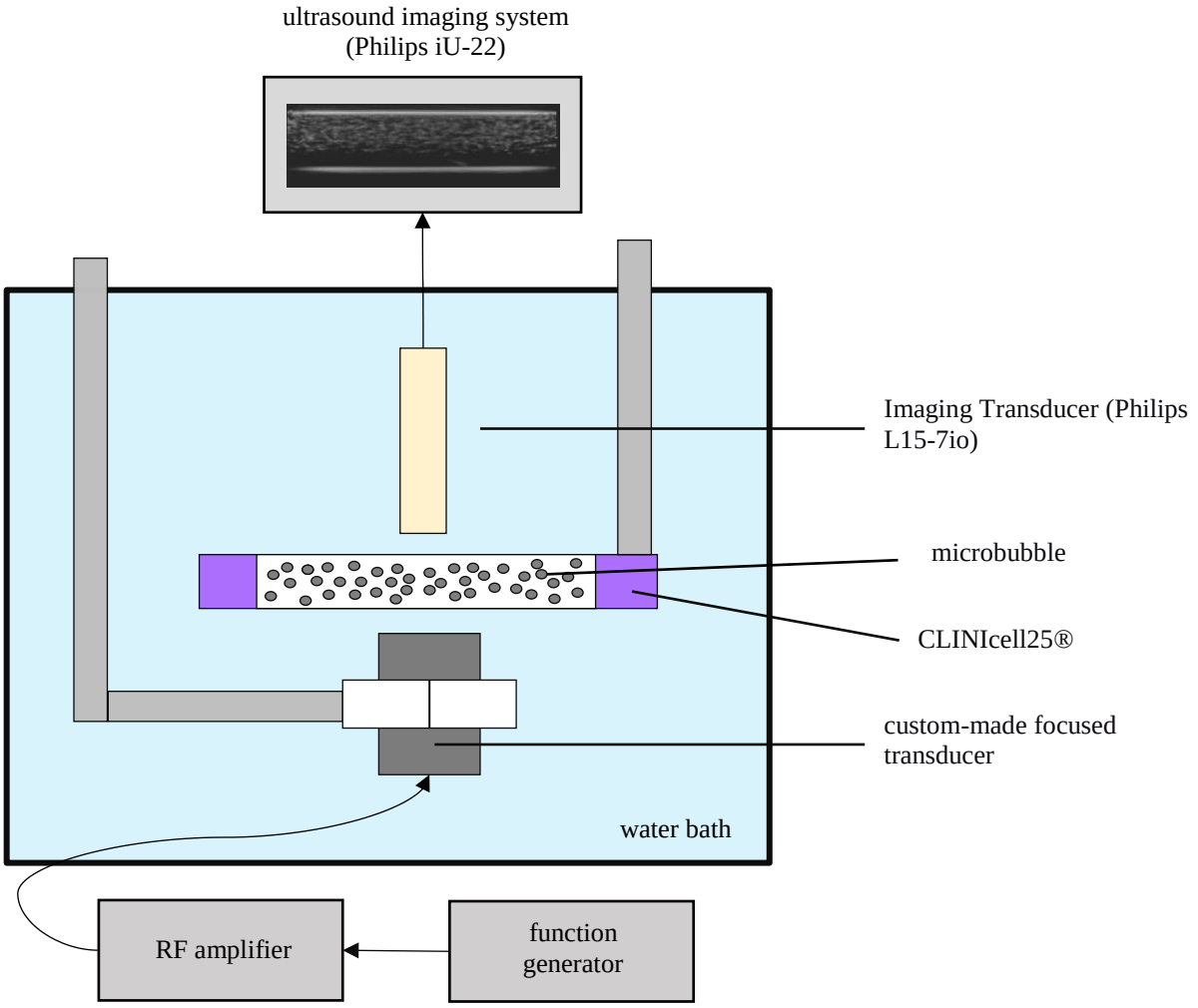

Figure 2.2. Instrument setup for observing microbubble behavior under the influence of ultrasound. A CLINIcell was placed in between a custom-made transducer and an imaging probe. An acoustic pulse was shot by the custom-made transducer while the whole process was imaged by diagnostic ultrasound.

2.5 SONOPORATION IN ACOUSTICALLY TRANSPARENT CELL CULTURE (CLINICELL)

As mentioned previously, this experiment was designed to evaluate the sonoporation efficiency of certain acoustic parameters and microbubble concentration. The experimental setup was similar to

the setup for the previous experiment and is shown in Figure 2.3. A GFP-HUVECs-seeded Clinicell was placed in between custom-made focused transducer (transducer frequency: 1 MHz; signal amplification at focus: 2.6; focal distance: 4 cm; diameter: 2 cm) and an imaging transducer (L15-7io linear array; Philips Healthcare, Bothell, WA, USA) in a water tank. The CLNIcell was positioned such that the area imaged by the imaging transducer was at the focus of the custom-made transducer. Adjustments were done with simple pulse-echo technique.

The experimental steps were the following: 1) Propidium Iodide (PI) (Thermo Fisher Scientific, Bothell, WA, USA) was added to CLINIcell ten minutes prior to the experiment at the final concentration of 10 µg/ml. PI was live-cell impermeable and can only enter cells with disrupted plasma membrane, and therefore it serves as our sonoporation marker. Once PI enters cells, it binds to DNA and RNA and emits red fluorescence. 2) Pre-exposure control images of the CLINIcell were taken with an inverted microscope (Nikon Instruments, Minato, Japan) (Figure 2.4). The CLINIcell was inspected for cell viability (with GFP fluorescence) and existing cell death (with PI fluorescence) at this stage. Four regions of interests (ROIs) were chosen for ultrasound exposure 3) The CLINIcell was exposed to ultrasound four times at the four selected ROIs. 4) Post-exposure images were taken at the four ROIs. 5) Through comparing pre-exposure images and post-exposure images, analysis of sonoporation efficiency was done with ImageJ [26].

In regard to the acoustic parameters tested, single pulse exposures were compared to repeated pulse (10% duty cycle, 5s exposure) exposures for sonoporation efficiency. Acoustic pressure (500 kPa) and pulse duration (1000 cycles) were kept constant. An experimental control was also included to verify that GFP-HUVECs do not allow spontaneous entry of PI and cellular membrane does not become permeabilized to PI naturally over time. This was done by adding PI to a CLINIcell without exposing it to ultrasound and examining the cells overtime.

Considering microbubble concentration, we hypothesized that the minimum microbubble concentration in CLINcell must achieve at least a 1:1 microbubble-to-cell ratio to produce sonoporation effectively. By accounting for the dimensions of a CLINIcell and estimating the microbubble distribution in CLINIcell, we calculated that the microbubble concentration must be at least 200,000 MBs/ml to achieve such a ratio. In this experiment, we tested two microbubble concentrations: 4×10^5 and 4×10^6 MBs/ml.

The GFP-HUVEC-seeded CLINIcells were prepared as following: 1) GFP-HUVECs in culture flasks were harvested with 0.05% trypsin-EDTA (ThermoFisher Scientific, Bothell, WA, USA) 2) CLINIcells were coated with collagen I (concentration: 10 μg/ml) and incubated for 2 hours. 3) GFP-HUVECs were added to CLINIcells and the devices were cultured in a 37°C, 5% CO_2 incubator until a cell monolayer grows to near-100% confluency.

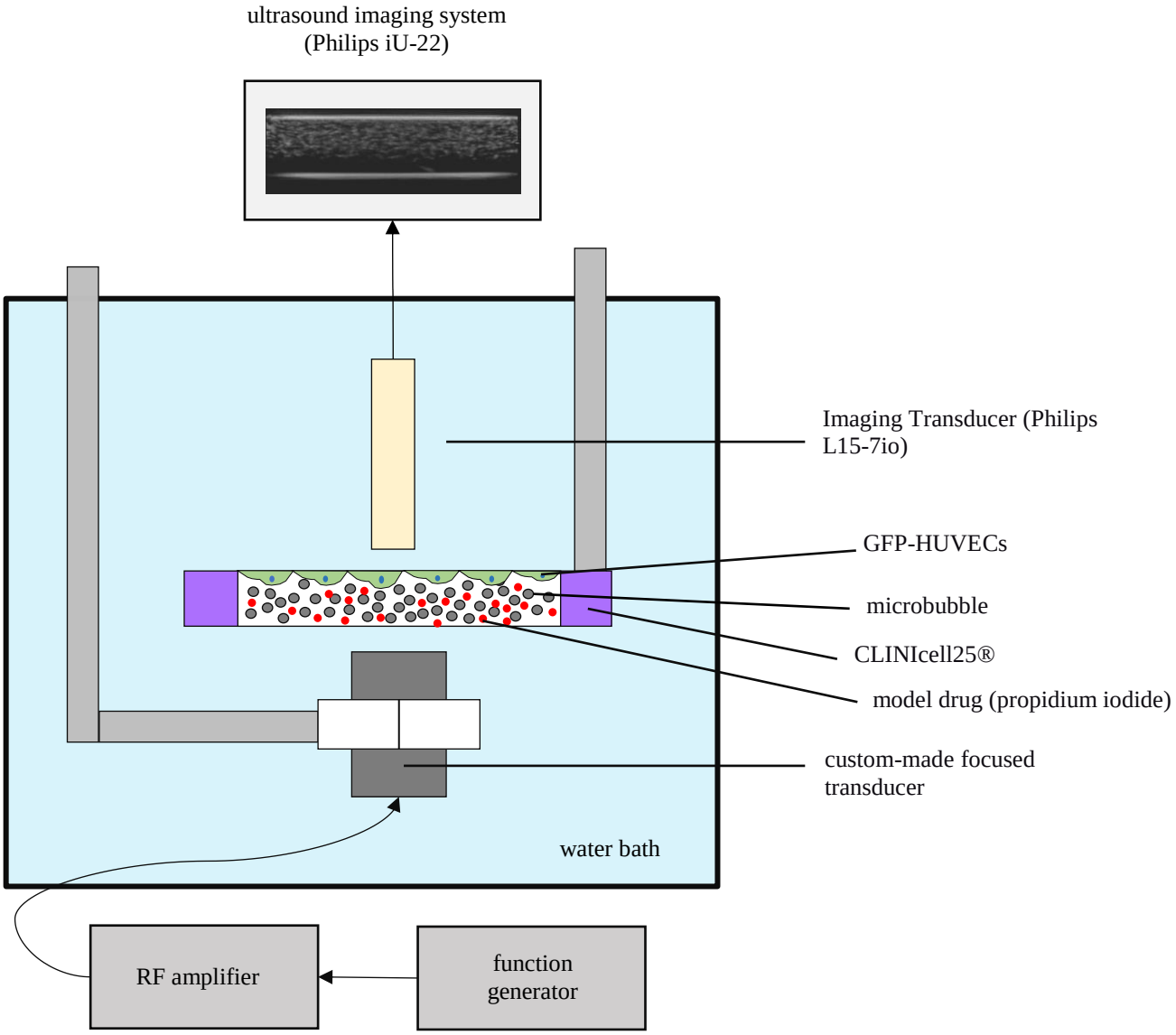

Figure 2.3. Schematic illustration of the experimental setup for sonoporation in CLINIcell. A CLINIcell seeded with GFP-HUVECs was placed in between a custom-made transducer and an imaging probe. The custom-made transducer sent a burst of ultrasound pulses to the microbubble filled CLINIcell to induce sonoporation. The imaging transducer produced B-mode images by sending pulses to and receiving pulses from the CLINICell.

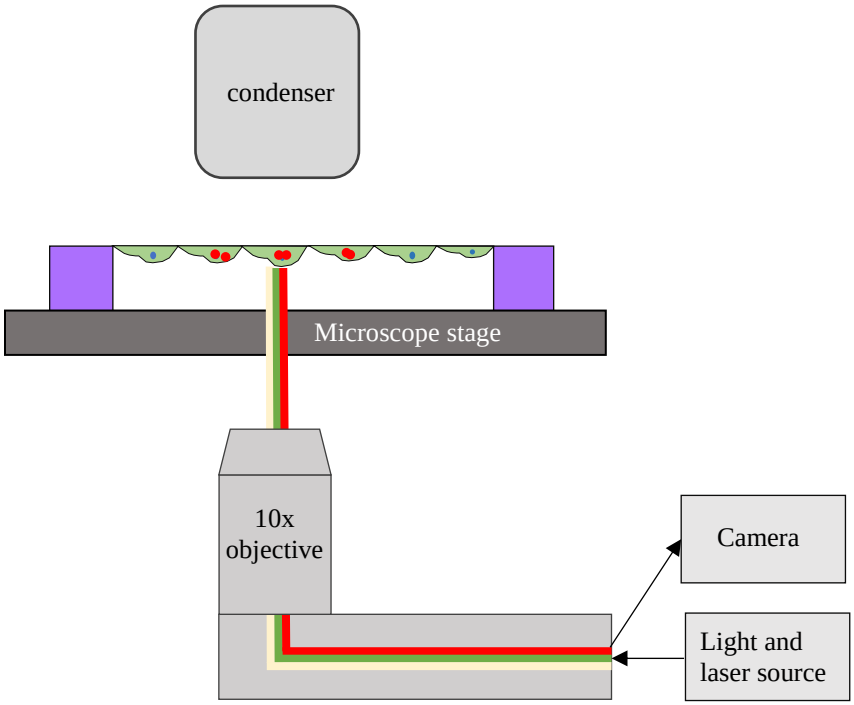

Figure 2.4. Illustration of the microscope setup to visualize sonoporation in CLINIcell. Before and after a cell-seeded CLINIcell loaded with microbubbles and propidium iodide was exposed to ultrasound, it was imaged with an inverted microscope. Bright-field images and fluorescence images of four selected region of interests were taken.

2.6 FABRICATION OF *IN VITRO* MICROVESSELS

Polydimethylsiloxane (PDMS) (Dow Corning, Midland, MI, USA) stamps were micropatterned with desired microvascular structures using microfabrication and soft lithography. Design of the microvascular pattern is shown in Figure 2.5. A schematic of the process of microbubble fabrication is shown in Figure 2.6. Type I collagen was extracted from rat tails and prepared to a stock concentration of 15 mg/ml. To make microvessels, type I collagen was diluted and neutralized to 7.5mg/ml on ice. Before each use, type I collagen was centrifuged at 1000g and 4ºC for 7 minutes to remove air bubbles. Liquid Type I collagen was injected into the space enclosed by the top acrylic housing of the and a micropatterned PDMS stamp; it was allowed to gel at 37ºC

for 30 minutes. The bottom half of the microvessel was prepared with a flat PDMS piece in a similar manner. After collagen has sufficiently gelled, the top and bottom pieces were assembled together to form a complete in vitro microvascular device. HUVECs (seeding concentration 7×10^6 cells/ml) were then injected into the microvessel through its inlet and outlet and allowed to attach to the microvascular wall. These cells were cultured with EGM under gravitational flow for four or more days before use.

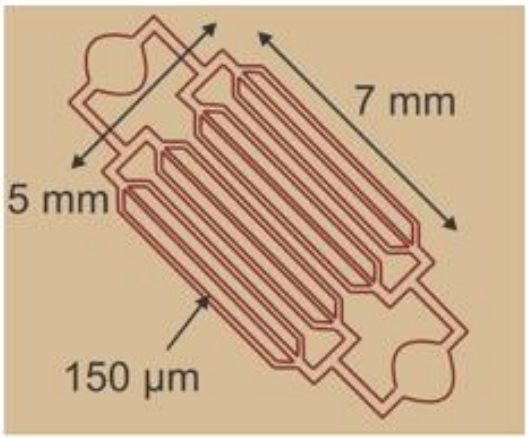

Figure 2.5. Illustration of the pattern of the in vitro microvascular model. The twelve parallel channels, each with a 150 μm width, simulate the small arterioles in human. This pattern was designed to have homogeneous flow profile from the inlet to the outlet and was micropatterned on to a PDMS stamp.

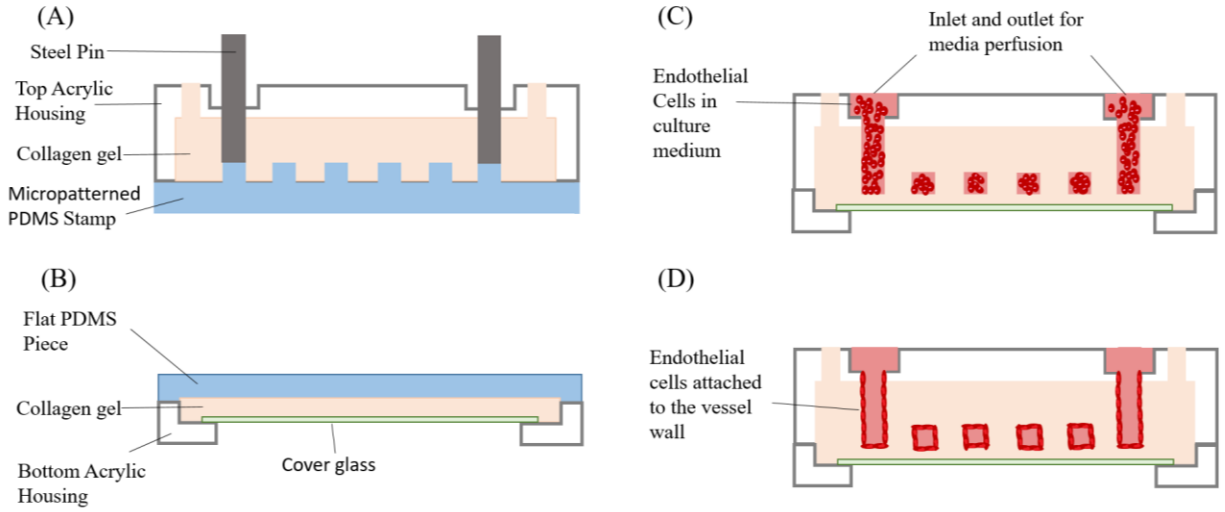

Figure 2.6. A schematic overview of the in vitro microvessel assembly and seeding procedures. (A) collagen I was injected into the space enclosed by the top acrylic housing and a micropatterned PDMS stamp in the top acrylic housing. (B) A thin layer of collagen was pressed with a flat PDMS piece to produce a flat collagen surface in the bottom acrylic housing. With collagen in place, the top and bottom jigs were incubated at 37ºC in a humidified chamber, allowing collgen to gel. (C) After collagen has sufficiently gelled, the top and bottom jigs were assembled together to form a complete in vitro microvascular device. HUVECs were injected into the device through pipetting and allowed to attach to the surface of the collagen-formed vascular lumens. (D) After two days of culture, HUVECs would attach and align into a tubular monolayer in the microvascular lumen. *The relative proportions of the components are not to scale.

2.7 SONOPORATION IN *IN VITRO* MICROVESSELS

This setup was used to study the efficacy of sonoporation in an in vivo-like environment. Prior to ultrasound exposure, HUVECs in the microvessels were incubated with Hoechst 33342 (Life Technologies, Carlsbad, CA, USA) (final concentration: 1 µg/ml) for 30 minutes. Hoechst 33342 was used to stain the nuclei of the cells in the vessel. Calcein-AM only fluoreces green in live cells and was therefore used as our viability marker to check.

During the experiment, a syringe pump (Cole-Parmer, Vernon Hills, IL, USA) was used to deliver PI (final concentration: 25 µg/ml) and microbubbles to the microvascular device through a silicone

tubing. A high microbubble concentration (final concentration: 1.5×10^8 MBs/ml) was used to allow more microbubble-vessel contact under flow condition. The prescribed flow rate was 0.2 ml/hr. This was selected to create physiological shear on the HUVECs in the microvascular device. A second silicone tubing removed flow-throughs from the outlet of the microvascular device. Immediately before ultrasound exposure, ultrasonic gel was applied to the top of the microvascular device. A custom-made transducer (transducer frequency: 1 MHz; signal amplification at focus: 2.6; focal distance: 4 cm; diameter: 2 cm) was held above the microvessel and used to sonicate the microvessel. Two sets of acoustic parameters were tested: 1) 1 MHz, 1.4 MPa, 500 cycles, 5% duty cycle, 5s exposure, and 2) 1 MHz, 400 kPa, 1000 cycles, 20% duty cycle, 5s exposure. The microvascular device was imaged with an inverted microscope before, during, and after ultrasound exposure. Image analysis and quantification were done with ImageJ [26].

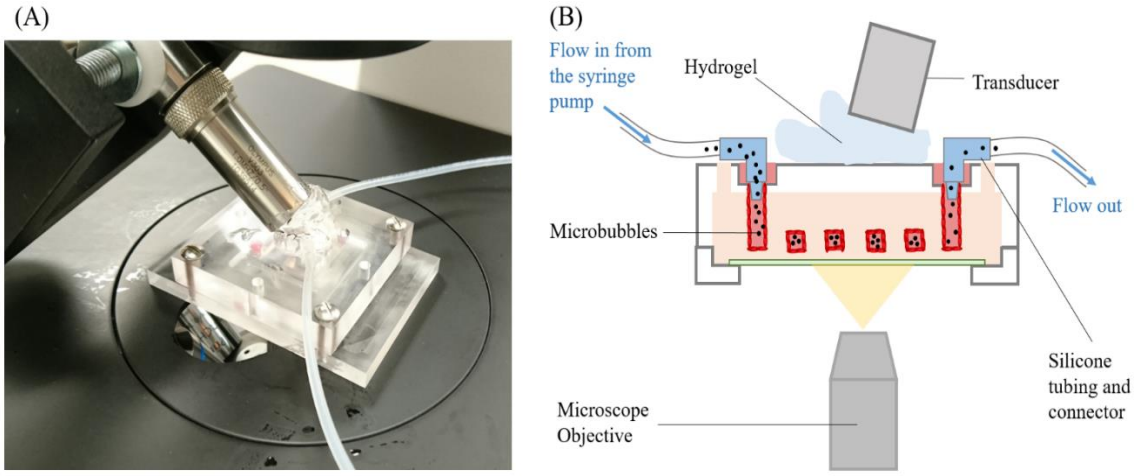

Figure 2.7. Picture (A) and schematic (B) of the experimental setup for sonoporation in in vitro microvessels. A silicone tubing directed flow (containing microbubbles) from the syringe pump into the microvessel model, and a second silicone tubing passively drained the flow-throughs from the outlet. Ultrasound gel was applied to the top of the acrylic enclosure, and the microvessel was

exposed to ultrasound to induce sonoporation. Videos and static bright-field and fluorescent images were acquired using an inverted microscope.

Chapter 3. RESULTS

3.1 ACOUSTIC ATTENUATION BY MICROBUBBLES

As ultrasound propagates through a thermos-viscous medium such as a microbubble solution, its energy (and therefore its amplitude) reduces due to scattering and absorption. This is referred to as acoustic attenuation. In the context of sonoporation, it is important to understand that the higher the microbubble concentration used and the further ultrasound propagates, the greater the ultrasound attenuation. This implies that the acoustic pressure experienced by the cells and the microbubbles near the cells will not be the same as the source acoustic pressure, and therefore, the ultrasound radiation force exerted on the cells and the amplitude and mode of microbubble cavitation may be different than what was expected from the prescribed conditions. Therefore, before attempting sonoporation in CLINIcells and in microvascular devices, we must first quantify acoustic attenuation at various microbubble concentrations.

A plot of normalized root mean square (RMS) voltage measurements as a function of microbubble concentration is shown in Figure 3.1. The RMS voltage measured was directly related to the peak negative pressure received by the needle hydrophone. Normalization was done with respect to the measurements obtained with CLINIcell filled with water, which was considered an acoustically lossless medium.

Looking at the overall trend, acoustic pressure decreased with increasing microbubble concentration as expected. As a reminder, the two ultrasound pulse settings compared in Figure 3.1 were 1) 1 MHz, 500 kPa, 20 cycles, single pulse, and 2) 1 MHz, 100 kPa, 20 cycles, single pulse, with the acoustic pressure being the only variant. Interestingly, the rate of attenuation seemed to depend on the source acoustic pressure. While the 500 kPa pulse attenuated almost

linearly with logarithmically increasing concentration, the 100 kPa pulse showed no attenuation until 1×10^5 MBs/ml, at which the pressure dropped dramatically. Another notable observation was that attenuation seemed to increase with increasing source pressure as the percentage loss in acoustic pressure for the 100 kPa pulse was consistently lower than that of the 500 kPa pulse. Still more to note was that a steep reduction in measured acoustic pressure was observed between 1×10^5 and 1×10^6 MBs/ml. Specifically, for the 100 kPa pulse, the remaining acoustic pressure decreased from 99% to 28% between 1×10^5 and 5×10^5 MBs/ml. For the 500 kPa pulse, the remaining acoustic pressure decreased from 42% to 13% in the same concentration interval. This trend agreed with the findings in literature that significant acoustic shadowing occurred beyond 4×10^5 MBs/ml [27]. As mentioned in section 2.5, the minimum required microbubble concentration to produce sonoporation effectively in CLINIcell was estimated at 2×10^5 MBs/ml. Our data, therefore, implied that if a microbubble concentration greater than the minimum required concentration was used to sonicate cells, the acoustic pressure experienced by the cells and microbubbles near the cells would be much less than the source pressure due to significant attenuation. Thus, pulse repetition or greater source pressure could be needed to compensate for acoustic attenuation if a high microbubble concentration was used.

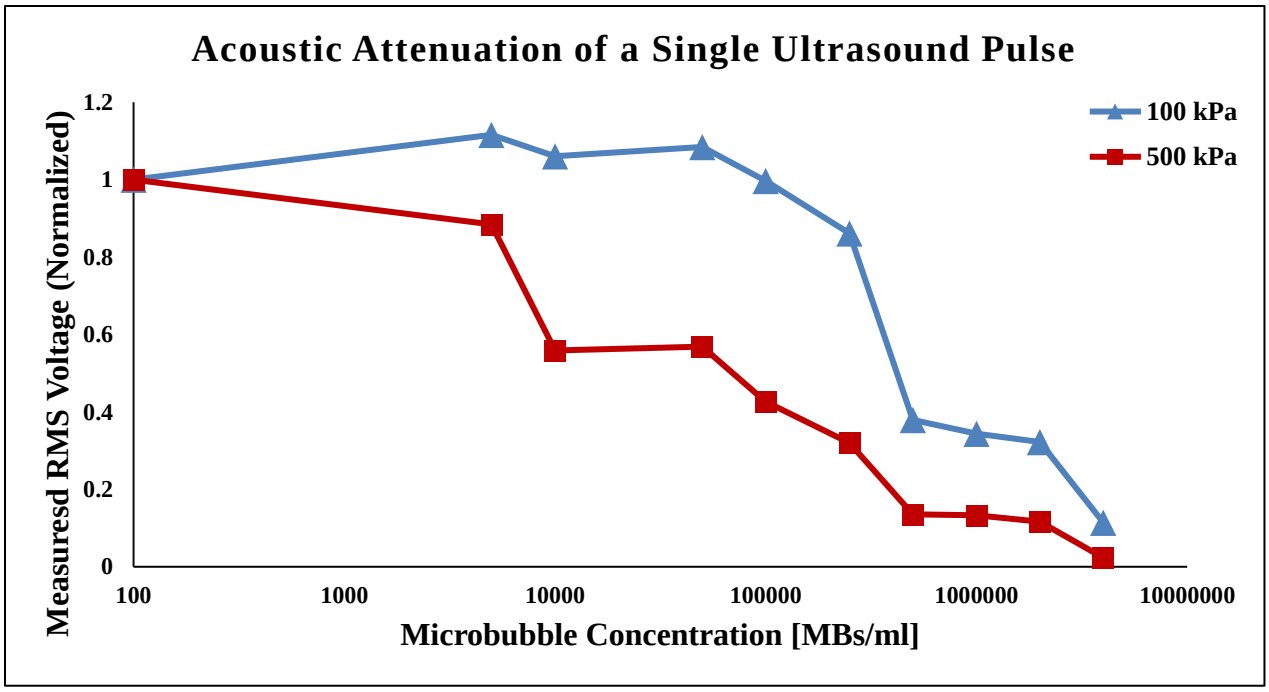

Figure 3.1. Ultrasound pulse amplitude (represented by RMS voltage) decreased with increased microbubble concentration. The plot showed the attenuation curves of two different ultrasound pulses: 1) 1 MHz, 100 kPa, 20 cycles, single pulse, and 2) 1 MHz, 500 kPa, 20 cycles, single pulse. The latter showed a faster decline than the former.

3.2 MICROBUBBLE BEHAVIOR IN ULTRASOUND

In addition to quantifying acoustic attenuation by microbubbles, we also examined the behavior of microbubbles in the presence of ultrasound with the setup described in section 2.4. In doing so, we aimed to identify certain microbubble behaviors that contribute to greater sonoporation, especially in the context of a static in vitro cell culture environment. Figure 3.2 shows the B-mode images of microbubble destruction and movement in CLINIcell in response to single ultrasound pulses. The single pulses varied only by pressure (200, 500, 1000 kPa) while the central transducer frequency (1 MHz) and pulse duration (1000 cycles) were kept constant. Image series A, B, and C (representing 200, 500, and 1000 kPa, respectively) demonstrated the destruction and movement of microbubbles in CLINIcell at 4×10^5 MBs/ml. As indicated by the increasing size of voids

created by ultrasound exposure, microbubbles destruction and the destruction range increased with increasing pressure. Additionally, more acoustic streaming and microbubble movement were observed at higher acoustic pressures. While pulse duration and pulse repetition were also factors that influence acoustic streaming and microbubble movement, since they were kept constant in the experiment, it was assumed that the increase in acoustic pressure alone led to increased acoustic streaming and microbubble movement. Another important observation was that the 200 kPa single pulse was not able to clear the microbubbles in its path to reach the top of the CLINIcell. This implied that the 200 kPa single pulse at 1000 cycles may have fully attenuated before it reached the top, which meant that the pulse may not have enough energy to produce sonoporation at the top of the CLINIcell. Contrarily, both the 500 kPa single pulse and the 1 MPa single pulse successfully cleared microbubbles in their paths. This suggested that the two pulses could both deliver sufficient energy to induce sonoporation. Since the 1 MPa pulse led to more intense microbubble destruction and acoustic streaming, we suspected that it may lead to more sonoporation than the 500 kPa pulse. B-mode image series D , E , F (representing 200, 500, and 1000 kPa, respectively) showed the destruction and movement of microbubbles in CLINIcell at 2×10^{6} MBs/ml. The observations regarding microbubble destruction, microbubble movement, and acoustic streaming were similar to the observations from A, B, and C. However, at five times the microbubble concentration, the voids created by ultrasound pulses in D, E, and F were noticeably smaller than the those seen in A, B, and C. While the sizes of the voids decreased, the 500 kPa pulse and the 1 MPa pulse still penetrated the microbubble layer in the CLINIcell and reached the top, indicating that these pulses may still have enough energy to induce sonoporation in a smaller area, despite attenuating more at a higher microbubble concentration. Based on the observations from this experiment, we hypothesized that to produce sonoporation with a single

ultrasound pulse in CLINIcell (and similar in vitro environment) the acoustic pressure used must be greater than 500 kPa. Moreover, given the literature suggestion that high acoustic pressure and violent microbubble movement could lead to irreversible perforation of cellular membrane and cell death, 1 MPa could be the maximum acoustic pressure to use since much microbubble movement and acoustic streaming were already observed at this pressure (refer to image series C and F) [18, 19, 21].

In selecting a set of ultrasound parameters for sonoporation in vitro, first, 500 kPa was chosen based on the observation that it was able to produce consistent and moderate microbubble destruction and movement. Regarding pulse duration, 1000 cycles was selected to prolong the ultrasound pulse to induce extensive microbubble mixing, translation, and inertial cavitation. In fact, 1000 cycles were sufficient to induce sonoporation without much cell death according to the literature [19]. Single ultrasound pulse was suggested instead of repeated pulses because it was already sufficient to destroy most microbubbles in the direct path of the pulse. Repeated pulse may not induce a greater impact since most microbubbles were destroyed after the initial pulse.

To summarize, we suspected that a single ultrasound pulse at 1 MHz, 500 kPa, 1000 cycles would be sufficient to produce effective sonoporation.

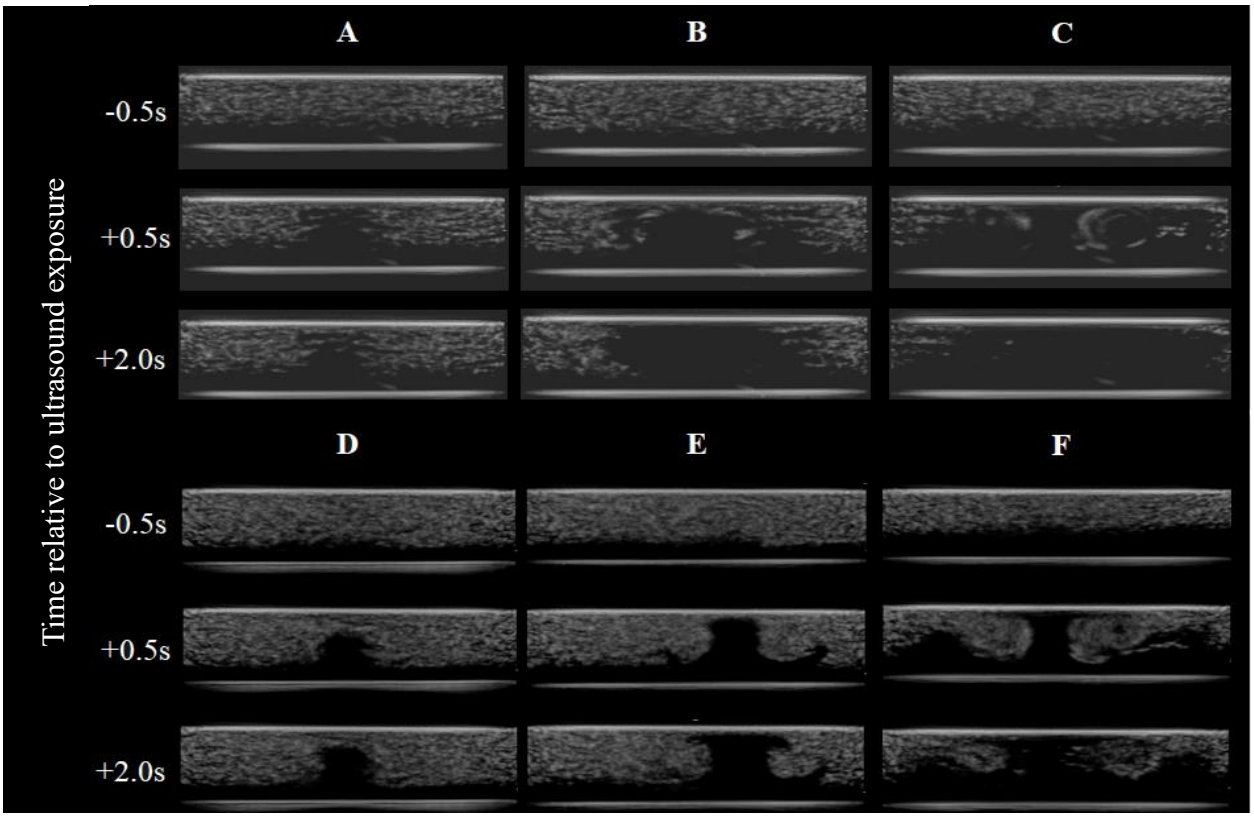

Figure 3.2. B-mode images of microbubble destruction and movement as responses to different acoustic pulses. A, B, and C are images of CLINICells filled with microbubbles at 4×10^5 MBs/ml before and after ultrasound exposure. D, E, and F are images of CLINICells filled with microbubbles at 2×10^6 MBs/ml before and after ultrasound exposure. CLINICells A and D were exposed to 200 kPa single ultrasound pulse; CLINICells B and E were exposed to 500 kPa single ultrasound pulse; CLINICell C and F were exposed to 1 MPa single ultrasound pulse. Transducer frequency (1 MHz) and pulse duration (1000 cycles) were held constant for all exposures. More microbubble destruction and acoustic streaming were observed with increased acoustic pressure.

3.3 SONOPORATION IN STATIC CELL CULTURE (CLINICELL)

We evaluated the sonoporation efficiency in CLINIcells based on the parameters determined in the previous section, and the results are shown in Figure 3.3. Column A represent an experimental control which PI was added to a CLINIcell but no ultrasound exposure was done. In fact, no signs of spontaneous uptake of PI in GFP-HUVECs were observed after 1.5 hours.

Column B shows the comparison of GFP-HUVECS in CLINIcell before and after exposure to a single ultrasound pulse at 1 MHz, 500 kPa, and 1000 cycles. Contrary to our expectation, very little sign of sonoporation was observed. While the total amount of PI in view varied before and after exposure, it is likely the result of the displacement of existing dead cells instead of sonoporation-induced cell death because PI signals were found outside of cells. In attempts to elicit a stronger mechanical effect on the GFP-HUVECs, we used a pulse repetition frequency of 100 Hz while keeping all other acoustic parameters constant. Specifically, the ultrasound parameters after adjustments were 1 MHz, 500 kPa, 1000 cycles, 10% duty cycle, and 5-second exposure. Duty cycle represents percentage of ultrasound operating time in a given period. To account for the microbubbles destroyed in each successively fired pulse, the microbubble concentration used was increased ten times, from 4×10^5 MBs/ml to 4×10^6 MBs/ml. Despite these changes, however, no observation of sonoporation was made (see column C).

While more experiments need to be done to confirm these results, they suggested that higher source pressure (> 500kPa), pulse duration (> 1000 cycles), pulse repetition frequency, microbubble concentration, or a combination of the four could be needed to induce effective sonoporation. This could very well be true in our microvascular model and in vivo, where microbubble-cell contact time was reduced due to flow and ultrasound scattering was increased due to more complexed geometries.

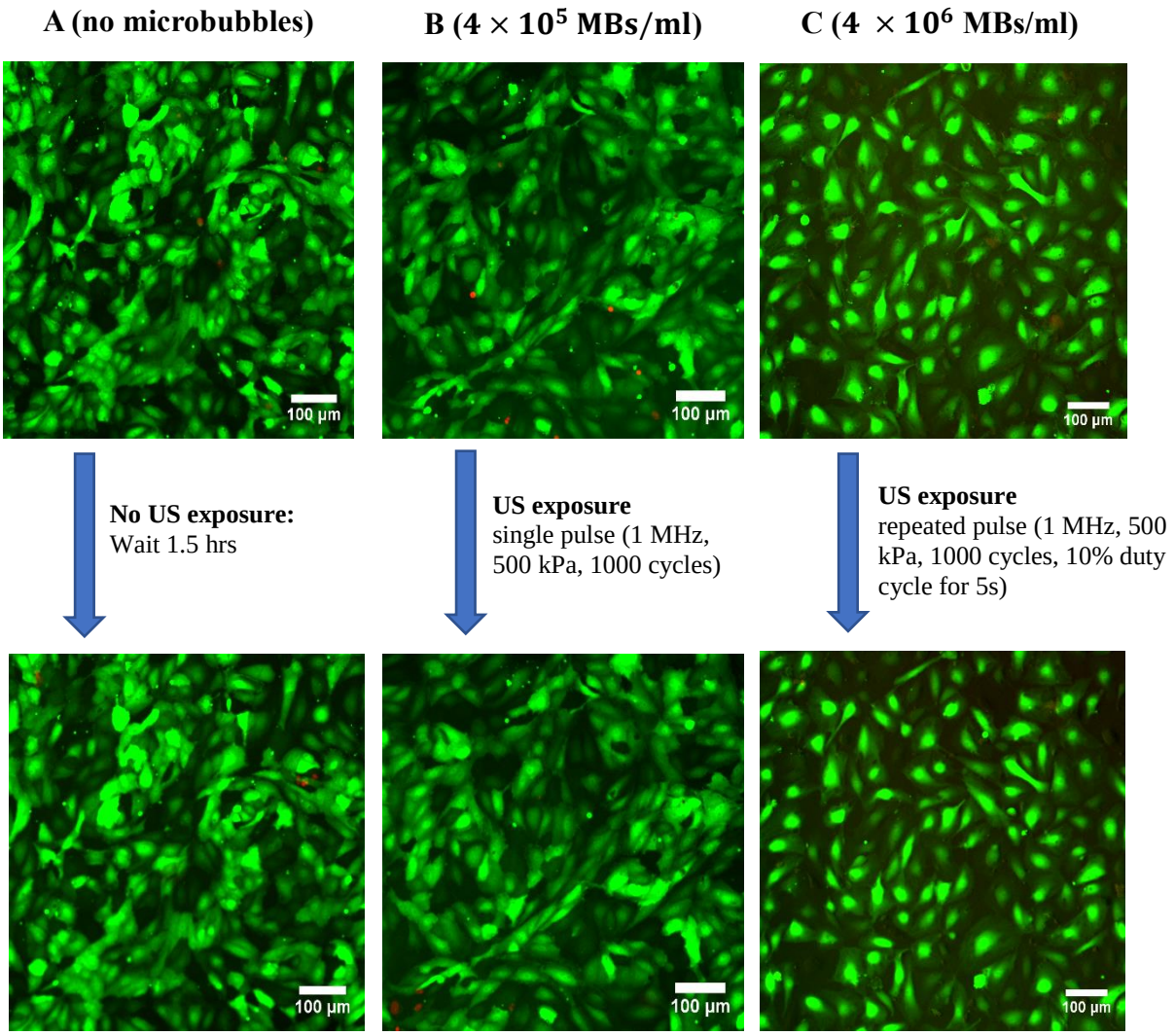

Figure 3.3. Image comparisons of GFP-HUVEC-seeded CLINICells before (first row) and after (second row) experimental maneuver. (A) showed an experimental control which only propidium iodide (PI) was added to the CLINIcell. This control served to verify that no PI spontaneously entered the HUVECs. (B) showed images of GFP-HUVECS before and after exposure to a single pulse ultrasound. (C) showed images of GFP-HUVECs before and after exposure to repeated ultrasound pulses. No PI uptake was observed in B and C. The green fluorescence in the images were GFPs in viable HUVECs. The red fluorescence was PI.

3.4 SONOPORATION IN AN *IN VIVO*-LIKE MICROVASCULAR ENVIRONMENT

To provide a more realistic human vascular model, our group has successfully fabricated an in vitro microvascular model that consisted of twelve parallel channels connected at the inlet and outlet (Figure 3.6). HUVECs injected into the microvessel covered the vascular lumen entirely and remained viable after 7 days of culture. This in vitro microvascular model allowed us to perfuse microbubbles into the vasculature and observe microbubble-vessel interaction in real-time with and without ultrasound.

Here, we compared the sonoporation efficiency of two sets of acoustic parameters 1) 1 MHz, 1.4 MPa, 500 cycles, 5% duty cycle, 5-second exposure, and 2) 1 MHz, 400 kPa, 1000 cycles, 20% duty cycle, 5-second exposure. Sonoporation efficiency was defined as the ratio of the total number of sonoporated cells to the total number of live cells. At a source pressure of 1.4 MPa, the first parameter set was intended to induce inertial cavitation of microbubbles and elicit a strong biomechanical impact on HUVECs. On the other hand, with a more modest source pressure at 400 kPa and longer pulse duration and pulse repetition frequency, the second parameter set was intended to primarily produce stable cavitation and microbubble translation, which were suggested in the literature to induce sonoporation through membrane tear [21]. Through comparing the sonoporation efficiency of the two parameter sets, we hoped to gain a better understanding of whether inertial cavitation or stable cavitation contribute more to sonoporation. Figure 3.4 shows microscope images of areas of the in vitro microvessels before and after they were exposed to ultrasound. More PI was uptaken by the HUVECs in the microvessel exposed to the ultrasound burst using the first set of parameters. Microvessels exposed using the second set of parameter barely showed any signs of sonoporation.

Quantified data is shown in Figure 3.5. The first parameter set led to $15.74 \pm 18.00\%$ sonoporation efficiency while the second parameters set led to 4.24 ± 8.22 %. This suggested that inertial cavitation could be the greater contributor to sonoporation, although further experiments were needed to delineate the effects of individual acoustic parameters (transducer frequency, acoustic pressure, pulse duration, and pulse repetition). Based on these results and given the acoustic parameters and microbubble concentration we used, the acoustic pressure and microbubble concentration needed to induce sonoporation in vivo could be much higher than expected from the results obtained with in previous in vitro studies. However, the results were not statistically significant due to the high variance of sonoporation efficiency among different microvessels exposed to ultrasound of the same acoustic parameters. Therefore, more repetitions of the experiment need to be done to confirm the results.

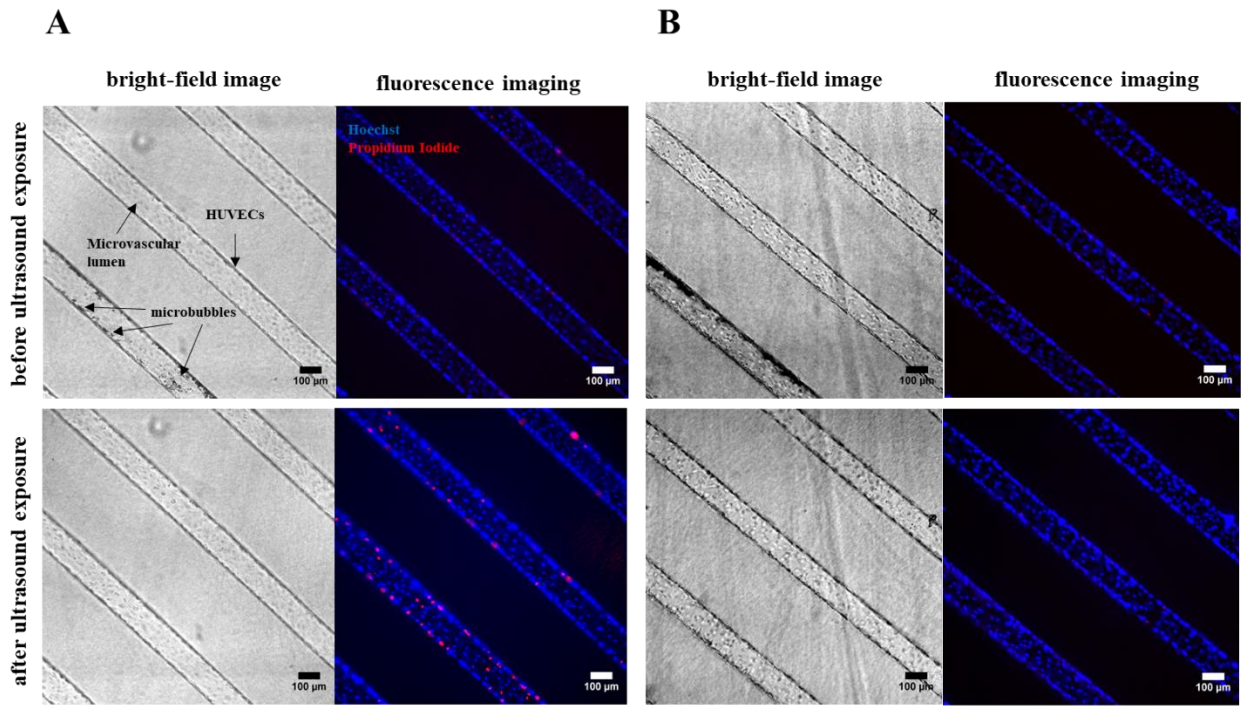

Figure 3.4. Bright-field and fluorescent image comparison of an area of an in vitro microvessel before and after ultrasound exposure. The extent of sonoporation in human-vessel-like environment is dependent on the acoustic pressure used. More evidence of

sonoporation was seen in in vitro microvessels exposed to 1 MHz, 1.4 MPa, 500 cycles, 5%DC ultrasound compared to 0.4 MPa, 500 cycles, 20%DC exposure. The top row shows images of a region of the microvessel taken before ultrasound exposure, and the bottom row shows images taken after ultrasound exposure. Hoechst 33342 (blue) stains the nuclei of the HUVECs in microvessels. Propidium iodide (red) binds to DNA and RNA of sonoporated cells.

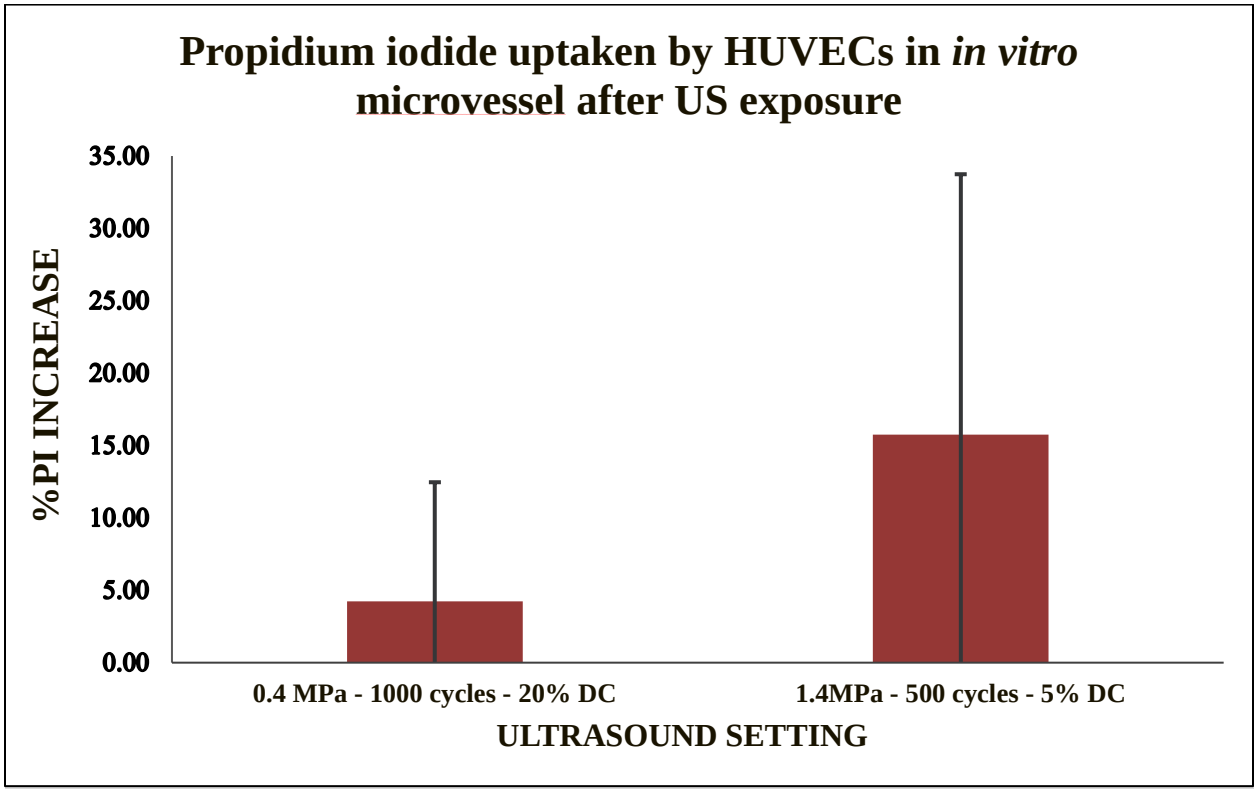

Figure 3.5. Propidium iodide uptake by HUVECs after sonoporation. Ultrasound at 1.4 MPa, 500 cycles, 5% duty cycle and 5s exposure induced about 15% sonoporation in HUVECs in the in vitro microvascular device, whereas ultrasound at 0.4 MPa, 1000 cycles, 20% duty cycle and 5s exposure induced only about 5%.

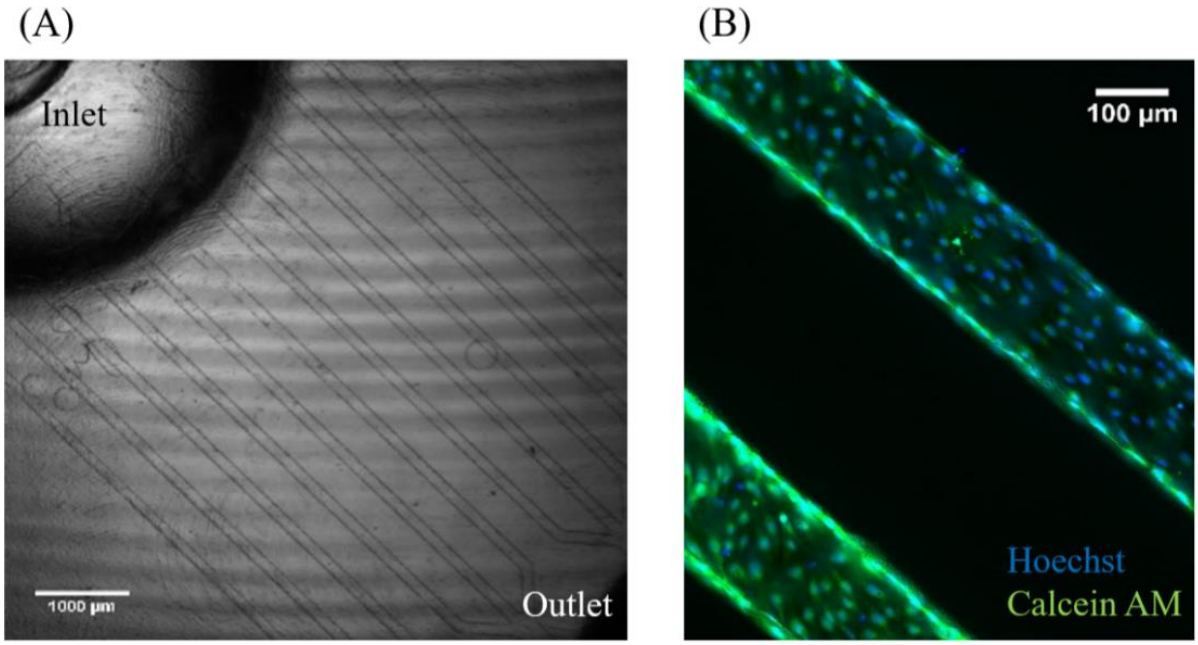

Figure 3.6. Bright-field and fluorescent images of an *in vitro* microvessel after 7 days of culture. (A) the HUVECs aligned nicely at the vessel wall. (B) Calcein AM and Hoechst staining together showed that the HUVECS attached to the vessel channels were still viable after 7 days of culture. Images were taken by an inverted microscope.

Chapter 4. DISCUSSIONS

4.1 DEPENDENCE OF SONOPORATION ON ACOUSTIC PRESSURE AND CELL TYPE

Despite vast efforts by various groups to study the feasibility of ultrasound and microbubble-mediated delivery in improving gene therapy and chemotherapy in vivo, very little consensus was reached as groups have reported varying levels of success [28-31]. In order to examine directly the microbubble-cell interaction in ultrasound and therefore identify the factors that influence sonoporation success, researchers have turned to in vitro platforms with windows observable by microscope. However, findings in the literature have been inconsistent as groups failed to agree

on the acoustic and non-acoustic parameters that would lead to sonoporation [17-20]. We believe part of the inconsistencies can be explained by the differences in experimental setups. In sonoporation studies which emphasized real-time microscopic observation of the cell-culture enclosures, the transducers were placed at an angle (mostly 45º) and sometimes arbitrary distance to the enclosures. This made it hard to determine the actual acoustic pressure delivered to the cells, especially in cases which focused transducers were used. To address this potential source of error, we used the experimental setup described in section 2.5 in our experiments. Although we sacrificed the opportunity to observe sonoporation real-time with this setup, we ensured that the acoustic pressure experienced by the cells were known, even accounting for acoustic attenuation. Regarding the culture devices, previous studies used a range of cell lines from human endothelial cells to fibroblasts to a variety of different cancer cell lines. While it may be beneficial to study the cells intended to be sonoporated in vivo, it is important to consider that different cell lines have variable susceptibilities to physical stimulus and could therefore exhibit varying levels of sonoporation when exposed to ultrasound and microbubbles [32]. In our experiments, we focused on endothelial cells because microbubbles come in contact with the vascular endothelium in the majority of the time they travel in the blood circulation.

Acoustic pressure is one of the most important contributing factors to sonoporation; it controls, most importantly among its many physical manifestations, the mode of microbubble cavitation (stable or inertial), the cavitation amplitude, and the size of pore generated on the cellular membrane [13, 17, 18, 33]. We reasoned that part of the inconsistencies in sonoporation efficiencies reported can be explained by the acoustic attenuation by microbubbles. Depending on the microbubble concentration used, cells and the microbubbles near the cells may experience very

different pressure amplitudes. As a part of this work, we evaluated the attenuation of acoustic pulse at the acoustic pressure (500 kPa) that has been reported to induce significant sonoporation.

According to Figure 3.1, at microbubble concentrations between 3×10^5 and 1×10^6 MBs/ml (concentrations used by us and others to achieve 1:1 microbubble-cell ratio), only 10 - 30% of acoustic pressure remained by the time a single pulse (1 MHZ, 500 kPa, 20 cycles) passed through a microbubble-filled CLINIcell. This implied that the actual pressure delivered to the cell monolayer was effectively only 50 – 150 kPa. Based on the ultrasound frequency (1 MHz) we used, these pressure values fell on both sides of the inertial cavitation threshold (about 100 kPa) of our custom-made microbubbles. If polymer-based microbubbles were used, these values would all fall below the cavitation threshold (about 200 kPa) at 1 MHz [33]. With sonoporation rate shown to depend on the inertial cavitation dose, it was no surprise that we did not observe much sonoporation at this source pressure (Figure 3.3) [32]. To increase the sonoporation efficiency at 500 kPa, one group increased the pulse duration of a single pulse and observed sonoporation of HUVECs from 1000 (10%) to 50,000 cycles (40%), although most of the cells were non-viable after exposure. Another group used repeated pulses (1 MHz, 500 kPa, 2000 cycles, 8% duty cycle, 5-second exposure) and achieved approximately 80% sonoporation efficiency in BLM-deficient epithelial cells at 4.4×10^6 MBs/ml, but they also observed a high amounts of cell debris at this ultrasound setting, possibly indicating massive cell death [17]. In contrast, we did not observe sonoporation in HUVECs with a similar pulse setting (1 MHZ, 500 kPa, 1000 cycles, 10% duty cycle, 5-second exposure) at a similar microbubble concentration (4×10^6 MBs/ml) (Figure 3.3). The difference in pulse duration could have made the deciding difference.

Experiments done with in vitro microvessels also revealed the dependence of sonoporation on acoustic pressure(Figure 3.5). Although the experiment only showed a qualitative comparison

between two sets of vastly different ultrasound parameters (refer to section 3.4), the set with higher acoustic pressure (1.4 MPa) produced significantly more sonoporation with lower acoustic pressure (0.4 MPa). In live-recordings of in vitro microvessels being exposed to ultrasound, it was observed that microbubbles imploded at the instant of the administration of the 1.4 MPa ultrasound burst, while most microbubble showed long distance translation and moderate destruction at 0.4 MPa. This again supported the findings that sonoporation is dependent on the inertial cavitation dose [33-34]. It is important to note that our in vitro microvascular model does not have an acoustically transparent window, and therefore the acoustic pressure delivered to the microvascular network is reduced from the source pressure.

4.2 THE USE OF IN VITRO MICROVASCULAR MODELS TO STUDY SONOPORATION

We are the first group to study sonoporation with a perfused in vitro microvascular model. Fabricated with native material (human endothelial cells and extracellular matrix) and designed to mimic human capillaries and small arterioles, our in vitro microvascular model captured important physiological features of the human vasculature and allowed us to study microbubble-cell interaction and sonoporation effects similar to they would happen in vivo. Additionally, our previous studies have demonstrated the possibility of co-culturing multiple cell types in the in vitro microvasculature [22]. With sufficient time cultured, it is also possible to observe angiogenesis within our microvascular model [22]. Finally, different microvascular network patterns can be designed and incorporated into our microvascular model to emulate healthy and unhealthy vessels found in the human body (Figure 4.1). These all leads to the possibility of creating a in vitro model that can mimic in vivo tumor.

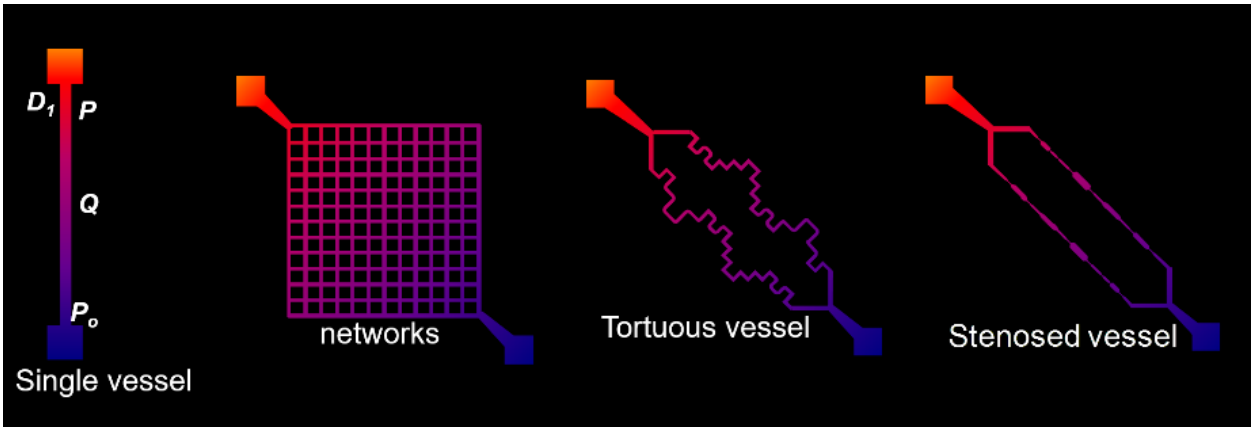

Figure 4.1. Different designs of microvascular network. The microvasculature in our device can be designed to emulate different vessel geometries found in the human body. Some existing designs shown here are large arterioles, capillary networks, tortuous vessels, and stenosed vessel.

Chapter 5. CONCLUSIONS

The interactions between ultrasound pulses and microbubble was examined for a range of different conditions. It was found that acoustic pressure attenuates dramatically in the microbubble concentration range of $1 \times 10^5 - 1 \times 10^6$ MBs/ml. In addition, microbubble destruction and the extent of acoustic streaming increase with acoustic pressure and decrease with microbubble concentration. In a static in vitro culture, HUVECs cannot be sonoporated at the acoustic pressure of 500 kPa with our single pulse (1 MHz, 1000 cycles) and repeated pulse (1 MHz, 1000 cycles, 10% duty cycle, 5-second exposure) setting. In vitro microvascular models are desirable as models for sonoporation studies. With this model, we observed $15.74 \pm 18.00\%$ sonoporation efficiency with the ultrasound sound condition of 1 MHz, 1.4 MPa, 500 cycles, 5% duty cycle and 5-second exposure, while a $4.24 \pm 8.22\%$ sonoporation efficiency was observed for 1 MHz, 0.4 MPa,

1000cycles, 20% duty cycle and 5-second exposure. Additional experiments need to be conducted for statistical significance. More work is needed to identify comparable conditions in vivo.

BIBLIOGRAPHY

1. S. Bao, B. D. Thrall, and D. L. Miller, "Transfection of a reporter plasmid into cultured cells by sonoporation in vitro," Ultrasound in Medicine & Biology, vol. 23, no. 6, pp. 953–959, 1997.

2. M.-L. D. Temmerman, H. Dewitte, R. E. Vandenbroucke, B. Lucas, C. Libert, J. Demeester, S. C. D. Smedt, I. Lentacker, and J. Rejman, "mRNA-Lipoplex loaded microbubble contrast agents for ultrasound-assisted transfection of dendritic cells," *Biomaterials*, vol. 32, no. 34, pp. 9128–9135, 2011.

3. V. Frenkel, "Ultrasound mediated delivery of drugs and genes to solid tumors," *Advanced Drug Delivery Reviews*, vol. 60, no. 10, pp. 1193–1208, 2008.

4. R. E. Vandenbroucke, I. Lentacker, J. Demeester, S. C. D. Smedt, and N. N. Sanders, "Ultrasound assisted siRNA delivery using PEG-siPlex loaded microbubbles," *Journal of Controlled Release*, vol. 126, no. 3, pp. 265–273, 2008.

5. J. Wu, J. Pepe, and M. Rincón, "Sonoporation, anti-cancer drug and antibody delivery using ultrasound," *Ultrasonics*, vol. 44, 2006.

6. K. Iwanaga, K. Tominaga, K. Yamamoto, M. Habu, H. Maeda, S. Akifusa, T. Tsujisawa, T. Okinaga, J. Fukuda, and T. Nishihara, "Local delivery system of cytotoxic agents to tumors by focused sonoporation," *Cancer Gene Therapy*, vol. 14, no. 4, pp. 354–363, Feb. 2007.

7. H. Maeda, K. Tominaga, K. Iwanaga, F. Nagao, M. Habu, T. Tsujisawa, Y. Seta, K. Toyoshima, J.-I. Fukuda, and T. Nishihara, "Targeted drug delivery system for oral cancer therapy using sonoporation," *Journal of Oral Pathology & Medicine*, vol. 38, no. 7, pp. 572–579, 2009.

8. K. Ferrara, R. Pollard, and M. Borden, "Ultrasound Microbubble Contrast Agents: Fundamentals and Application to Gene and Drug Delivery," *Annual Review of Biomedical Engineering*, vol. 9, no. 1, pp. 415–447, 2007.

9. S. R. Sirsi and M. A. Borden, "Microbubble compositions, properties and biomedical applications," *Bubble Science, Engineering & Technology*, vol. 1, no. 1-2, pp. 3–17, 2009.

10. R. Karshafian, P. D. Bevan, R. Williams, S. Samac, and P. N. Burns, "Sonoporation by Ultrasound-Activated Microbubble Contrast Agents: Effect of Acoustic Exposure Parameters on Cell Membrane Permeability and Cell Viability," *Ultrasound in Medicine & Biology*, vol. 35, no. 5, pp. 847–860, 2009.

11. E. Quaia, M. D'Onofrio, A. Palumbo, S. Rossi, S. Bruni, and M. Cova, "Comparison of contrast-enhanced ultrasonography versus baseline ultrasound and contrast-enhanced computed tomography in metastatic disease of the liver: diagnostic performance and confidence," *European Radiology*, vol. 16, no. 7, pp. 1599–1609, 2006.

12. J. Collis, R. Manasseh, P. Liovic, P. Tho, A. Ooi, K. Petkovic-Duran, and Y. Zhu, "Cavitation microstreaming and stress fields created by microbubbles," *Ultrasonics*, vol. 50, no. 2, pp. 273–279, 2010.

13. I. Lentacker, I. D. Cock, R. Deckers, S. D. Smedt, and C. Moonen, "Understanding ultrasound induced sonoporation: Definitions and underlying mechanisms," *Advanced Drug Delivery Reviews*, vol. 72, pp. 49–64, 2014.
14. X. Chen, R. S. Leow, Y. Hu, J. M. F. Wan, and A. C. H. Yu, "Single-site sonoporation disrupts actin cytoskeleton organization," *Journal of The Royal Society Interface*, vol. 11, no. 95, pp. 20140071–20140071, 2014.

15. A. Delalande, C. Leduc, P. Midoux, M. Postema, and C. Pichon, "Efficient Gene Delivery by Sonoporation Is Associated with Microbubble Entry into Cells and the Clathrin-Dependent Endocytosis Pathway," *Ultrasound in Medicine & Biology*, vol. 41, no. 7, pp. 1913–1926, 2015.

16. G. J. Czarnota, R. Karshafian, P. N. Burns, S. Wong, A. A. Mahrouki, J. W. Lee, A. Caissie, W. Tran, C. Kim, M. Furukawa, E. Wong, and A. Giles, "Tumor radiation response enhancement by acoustical stimulation of the vasculature," *Proceedings of the National Academy of Sciences*, vol. 109, no. 30, Sep. 2012.

17. I. D. Cock, E. Zagato, K. Braeckmans, Y. Luan, N. D. Jong, S. C. D. Smedt, and I. Lentacker, "Ultrasound and microbubble mediated drug delivery: Acoustic pressure as determinant for uptake via membrane pores or endocytosis," *Journal of Controlled Release*, vol. 197, pp. 20–28, 2015.

18. T. V. Rooij, I. Skachkov, I. Beekers, K. R. Lattwein, J. D. Voorneveld, T. J. Kokhuis, D. Bera, Y. Luan, A. F. V. D. Steen, N. D. Jong, and K. Kooiman, "Viability of endothelial cells after ultrasound-mediated sonoporation: Influence of targeting, oscillation, and displacement of microbubbles," *Journal of Controlled Release*, vol. 238, pp. 197–211, 2016.

19. B. Helfield, X. Chen, S. C. Watkins, and F. S. Villanueva, "Biophysical insight into mechanisms of sonoporation," *Proceedings of the National Academy of Sciences*, vol. 113, no. 36, pp. 9983–9988, 2016.

20. Y. Hu, J. M. Wan, and A. C. Yu, "Membrane Perforation and Recovery Dynamics in Microbubble-Mediated Sonoporation," *Ultrasound in Medicine & Biology*, vol. 39, no. 12, pp. 2393–2405, 2013.

21. P. Qin, L. Xu, T. Han, L. Du, and A. C. Yu, "Effect of non-acoustic parameters on heterogeneous sonoporation mediated by single-pulse ultrasound and microbubbles," *Ultrasonics Sonochemistry*, vol. 31, pp. 107–115, 2016.

22. Y. Zheng, J. Chen, M. Craven, N. W. Choi, S. Totorica, A. Diaz-Santana, P. Kermani, B. Hempstead, C. Fischbach-Teschl, J. A. Lopez, and A. D. Stroock, "In vitro microvessels for the study of angiogenesis and thrombosis," *Proceedings of the National Academy of Sciences*, vol. 109, no. 24, pp. 9342–9347, 2012.

23. Y. Zheng, J. Chen, and J. A. López, "Flow-driven assembly of VWF fibres and webs in in vitro microvessels," *Nature Communications*, vol. 6, p. 7858, 2015.

24. G. Ligresti, R. J. Nagao, J. Xue, Y. J. Choi, J. Xu, S. Ren, T. Aburatani, S. K. Anderson, J. W. Macdonald, T. K. Bammler, S. M. Schwartz, K. A. Muczynski, J. S. Duffield, J. Himmelfarb, and Y. Zheng, "A Novel Three-Dimensional Human Peritubular Microvascular System," *Journal of the American Society of Nephrology*, vol. 27, no. 8, pp. 2370–2381, Nov. 2015.

25. M.-L. D. Temmerman, H. Dewitte, R. E. Vandenbroucke, B. Lucas, C. Libert, J. Demeester, S. C. D. Smedt, I. Lentacker, and J. Rejman, "mRNA-Lipoplex loaded microbubble contrast agents for ultrasound-assisted transfection of dendritic cells," *Biomaterials*, vol. 32, no. 34, pp. 9128–9135, 2011.

26. J. Schindelin, I. Arganda-Carreras, E. Frise, V. Kaynig, M. Longair, T. Pietzsch, S. Preibisch, C. Rueden, S. Saalfeld, B. Schmid, J.-Y. Tinevez, D. J. White, V. Hartenstein, K. Eliceiri, P. Tomancak, and A. Cardona, "Fiji: an open-source platform for biological-image analysis," Nature Methods, vol. 9, no. 7, pp. 676–682, 2012.

27. M. Lampaskis and M. Averkiou, "Investigation of the Relationship of Nonlinear Backscattered Ultrasound Intensity with Microbubble Concentration at Low MI," *Ultrasound in Medicine & Biology*, vol. 36, no. 2, pp. 306–312, 2010.

28. Y. S. Li, E. Davidson, C. N. Reid, and A. P. Mchale, "Optimising ultrasound-mediated gene transfer (sonoporation) in vitro and prolonged expression of a transgene in vivo: Potential applications for gene therapy of cancer," *Cancer Letters*, vol. 273, no. 1, pp. 62–69, 2009.

29. P. Haag, F. Frauscher, J. Gradl, A. Seitz, G. Schäfer, J. R. Lindner, A. L. Klibanov, G. Bartsch, H. Klocker, and I. E. Eder, "Microbubble-enhanced ultrasound to deliver an

antisense oligodeoxynucleotide targeting the human androgen receptor into prostate tumours," *The Journal of Steroid Biochemistry and Molecular Biology*, vol. 102, no. 1-5, pp. 103–113, 2006.

30. L. C. Phillips, A. L. Klibanov, B. R. Wamhoff, and J. A. Hossack, "Targeted Gene Transfection from Microbubbles into Vascular Smooth Muscle Cells Using Focused, Ultrasound-Mediated Delivery," *Ultrasound in Medicine & Biology*, vol. 36, no. 9, pp. 1470–1480, 2010.

31. J. Escoffre, A. Novell, J. Piron, A. Zeghimi, A. Doinikov, and A. Bouakaz, "Microbubble attenuation and destruction: are they involved in sonoporation efficiency?," *IEEE Transactions on Ultrasonics, Ferroelectrics and Frequency Control*, vol. 60, no. 1, 2013.

32. S. Pichardo, M. Togtema, R. Jackson, I. Zehbe, and L. Curiel, "Influence of cell line and cell cycle phase on sonoporation transfection efficiency in cervical carcinoma cells under the same physical conditions," *IEEE Transactions on Ultrasonics, Ferroelectrics and Frequency Control*, vol. 60, no. 2, pp. 432–435, 2013.

33. C.-Y. Lai, C.-H. Wu, C.-C. Chen, and P.-C. Li, "Quantitative relations of acoustic inertial cavitation with sonoporation and cell viability," *Ultrasound in Medicine & Biology*, vol. 32, no. 12, pp. 1931–1941, 2006.

34. W.-S. Chen, T. J. Matula, A. A. Brayman, and L. A. Crum, "A comparison of the fragmentation thresholds and inertial cavitation doses of different ultrasound contrast agents," *The Journal of the Acoustical Society of America*, vol. 113, no. 1, pp. 643–651, 2003.